JMB

The Structure of Holo and Metal-deficient Wild-type Human Cu, Zn Superoxide Dismutase and its Relevance to Familial Amyotrophic Lateral Sclerosis

Richard W. Strange[1], Svetlana Antonyuk[1], Michael A. Hough[1] Peter A. Doucette[2], Jorge A. Rodriguez[2], P. John Hart[3] Lawrence J. Hayward[4], Joan S. Valentine[2] and S. Samar Hasnain[1]*

[1]*Molecular Biophysics Group Department of Synchrotron Radiation, CCLRC Daresbury Laboratory, Warrington Cheshire WA4 4AD, UK*

[2]*Department of Chemistry and Biochemistry, University of California, Los Angeles, CA 90095, USA*

[3]*X-ray Crystallography Core Laboratory, Department of Biochemistry, University of Texas Health Science Center San Antonio, 7703 Floyd Curl Drive, San Antonio, TX 78229-3900, USA*

[4]*Department of Neurology University of Massachusetts Medical School, 55 Lake Avenue North, Worcester, MA 01655, USA*

*Corresponding author

Cu, Zn superoxide dismutase (SOD1) forms a crucial component of the cellular defence against oxidative stress. Zn-deficient wild-type and mutant human SOD1 have been implicated in the disease familial amyotrophic lateral sclerosis (FALS). We present here the crystal structures of holo and metal-deficient (apo) wild-type protein at 1.8 Å resolution. The P21 wild-type holo enzyme structure has nine independently refined dimers and these combine to form a "trimer of dimers" packing motif in each asymmetric unit. There is no significant asymmetry between the monomers in these dimers, in contrast to the subunit structures of the FALS G37R mutant of human SOD1 and in bovine Cu,Zn SOD. Metal-deficient apo SOD1 crystallizes with two dimers in the asymmetric unit and shows changes in the metal-binding sites and disorder in the Zn binding and electrostatic loops of one dimer, which is devoid of metals. The second dimer lacks Cu but has ~20% occupancy of the Zn site and remains structurally similar to wild-type SOD1. The apo protein forms a continuous, extended arrangement of β-barrels stacked up along the short crystallographic *b*-axis, while perpendicular to this axis, the constituent β-strands form a zig-zag array of filaments, the overall arrangement of which has a similarity to the common structure associated with amyloid-like fibrils.
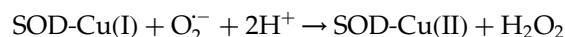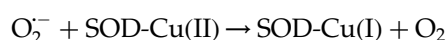
© 2003 Elsevier Science Ltd. All rights reserved

Keywords: Cu, Zn superoxide dismutase; familial amyotrophic lateral sclerosis; ALS, amyloid; SOD1

Introduction

Cytosolic Cu, Zn superoxide dismutase (SOD1; EC 1.15.1.1) is a critical component of the cellular defence against reactive oxygen species and catalyses the dismutation reaction of the superoxide radical anion to hydrogen peroxide and oxygen *via* the cyclic reduction and reoxidation of copper:[1]

$$O_2^{\cdot -} + SOD\text{-}Cu(II) \rightarrow SOD\text{-}Cu(I) + O_2$$

$$SOD\text{-}Cu(I) + O_2^{\cdot -} + 2H^+ \rightarrow SOD\text{-}Cu(II) + H_2O_2$$

SOD1 is found in all eukaryotic species as a homodimeric enzyme of ~32 kDa containing one Cu and one Zn ion per subunit. The overall fold in each subunit is described as an eight-stranded antiparallel β-barrel connected by three external loops.[2] Two of these loops, the Zn loop and the electrostatic loop, form the walls of a channel from the enzyme surface to the active site. The third loop region provides the Greek key connection across the β-barrel. Several charged residues within the electrostatic loop as well as

the catalytically important Arg143 are involved in the electronic guidance of the substrate to the active site and so contribute to the high-level specificity of SOD1 for the superoxide substrate.[3] The Zn loop is so named because it contains ligands for the Zn ion.

The metal ions in SOD1 are bridged by the imidazole ring of residue His63, which acts as a ligand to both metals. The Cu(II) is further coordinated to three histidine residues (46, 48 and 120) and a water molecule to form a distorted square pyramidal geometry, while the Zn coordination is completed by a further two histidine residues (71 and 80) and an aspartate residue (83) in a distorted tetrahedral geometry.[2] There is structural evidence from crystallography and EXAFS that the Cu-His63-Zn-bridge in SOD1 is broken upon reduction to Cu(I), leaving an approximate trigonal planar Cu coordination.[4–9]

Mutations in SOD1 have been associated with the development of amyotrophic lateral sclerosis (ALS),[10] a disorder affecting the integrity of motor neurons in the brain and spinal cord, leading to paralysis and death, usually within five years.[11] Some 10% of ALS cases are familial (FALS), and dominant inheritance of point mutations in SOD1 has been implicated in about 20% of FALS cases.[10,11] Normal enzymatic activity is often undiminished by the mutations, yet these changes impart a presently unidentified toxic property to the protein.[12–18] The nature of mutant SOD1 toxicity in FALS may be related to altered metal ion binding or to abnormal interactions of mutant SOD1 with itself or other cellular constituents.[19]

The mutations are scattered throughout the SOD1 gene that encodes the protein and they can lead to destabilization of the protein and a change in the metal-binding properties at the Zn-binding site compared to wild-type SOD1 [wtSOD1].[20–22] UV–visible spectroscopic studies of ALS equivalent mutations in yeast Cu, Zn SOD have shown similar results, and it has been suggested that ALS mutations may result in destabilization affecting the Zn affinity of the enzyme and that this, in turn, may result in a protein that is less stable and more prone to aggregation and denaturation than wild-type protein.[23] Zn-deficient wtSOD1 together with four ALS mutants were associated with motor neuron death *in vitro*, whereas their fully metallated counterparts were non-toxic.[20,24–26]

A mechanism for the toxic gain of function is provided by the idea that aggregation of misfolded mutant SOD1 protein is involved. Accumulation of mutant SOD1 containing aggregates has been observed in transgenic mouse models of the disease.[27–29] Abnormal aggregation of mutant SOD1 protein and apoptotic cell death were observed in culture models of mutant SOD1-expressing motor neurons.[30]

In contrast to the familial form of the disease, 90% of ALS cases occur through as yet unknown causes. These cases are termed sporadic ALS (SALS), and occur without the presence of known SOD1 mutations. It remains possible, however, that wild-type SOD1 expression could be relevant to motor neuron degeneration in some of these cases.[31,32] Because wild-type SOD1 is abundant in the cell bodies and processes of spinal motor neurons,[33] and has been detected in the inter-membrane space of mitochondria in liver cells,[34] further work on the wild-type protein in the context of ALS is warranted.

In light of the above, the structure of a Zn-deficient wtSOD1 protein is of considerable interest, and we present the first crystal structure of apo wtSOD1, at 1.82 Å resolution. The crystal possesses two dimers per asymmetric unit, one of which is completely free of metal, while the second dimer is Cu-free but contains ~20% of its normal Zn quota. This structure provides a possible insight into the structural and functional effects of FALS mutations. In particular, we show that metal-deficiency in wtSOD1 can lead to self-organization of the wild-type protein into an amyloid-like fibrillar structure. The formation of this fibrillar structure is dependent upon SOD1-SOD1 protein–protein interactions that are made possible through disorder in the Zn and electro-static loop elements of metal-free SOD1 subunits. We recently solved the crystal structures of three distinct FALS mutant species, the metal-depleted S134N, apo-H46R and Zn-H46R proteins, most of which possess similar fibrillar crystal packing arrangements.[35] We present a crystal structure for holo wtSOD1 at 1.78 Å resolution in space group $P2_1$. Two earlier crystal structures, a recombinant wtSOD1 and a thermostable double mutant Cys6Ala-Cys111Ser (PDB codes 1spd and 1sos, respectively) were reported at 2.4 Å and 2.5 Å resolution, respectively.[11,36] The modest resolution of these structures has hampered, to some extent, the analysis of mutant structures and the understanding of the structure–function relationships in this protein. The higher-resolution data in the present case have allowed accurate independent refinement of each of the dimeric molecules in the asymmetric unit, and an improvement in the accuracy of the atomic coordinates. This improvement in the quality of the structure for the wild-type human enzyme provides the much needed accuracy required to assess any changes that occur in the SOD1 structure as a result of the FALS mutations.

Results and discussion

Quality of the models

The wtSOD1 holo enzyme

The wtSOD1 model has been refined to an R-factor of 18.5% for all data in the resolution range 50–1.78 Å, excluding 5.0% of randomly distributed reflections assigned to calculate an R_{free} of 22.2% (Table 1). The asymmetric unit contains 18 subunits or nine functional dimers (here called

Table 1. Data collection and refinement statistics for holo and apo wtSOD1

Space group	*P*21	*C*2
Name of the sample	Holo	Apo
Number of dimers	9	2
Solvent content (%)	46	45
Resolution range (Å)	50.0–1.78	50–1.82
(Last shell)	(1.86–1.78)	(1.89–1.82)
Completeness (%)	98.6 (96.3)	96.1 (83.6)
R_{merge}[a]	5.2	6.1
$\langle I \rangle / \sigma I$ last shell	2.7	2.8
Redundancy	3.4 (3.0)	3.5 (3.0)
Overall reflections	904,897	176,234
Unique reflections	265,996	50,360
Wilson *B*-factor (Å^2)	26	26
Unit cell parameters		
a (Å)	76.8	156.4
b (Å)	172.3	34.9
c (Å)	112.5	114.8
α (deg.)	90	90
β (deg.)	93.5	112.26
γ (deg.)	90	90
Final R_{cryst}[b] (%)	18.5	23.2
R-free[c] (%)	22.2	28.2
ESU (Å) based on *R* value[d]	0.12	0.17
Number of atoms	21,664	4310
Number of water molecules	1099	323
Number of Ca ions	4	0
Average *B*-factor (Å^2) before TLS	31.8	46.0
Average *B*-factor (Å^2) after TLS	20.2	27.5

Figures in parentheses refer to outermost resolution shell.
[a] $R_{merge} = \sum |I_{hkl} - \langle I_{hkl} \rangle| / \sum I_{hkl}$.
[b] $R_{cryst} = \sum |F_{obs} - F_{calc}| / \sum F_{obs}$.
[c] R_{free} is the *R*-factor calculated from a subset of reflections excluded from refinement.
[d] ESU, estimated standard uncertainty as implemented in REFMAC.

A + H, B + I, C + J, D + K, E + L, F + M, G + N, O + Q and P + S). The nine dimers had average *B*-factors ranging from 25 to 50 Å^2, indicating their individual levels of disorder, related to their position in the crystal lattice. The electron density allowed the positioning of all 153 residues in each monomer. The final model contains 20,524 protein atoms, four Ca, 18 Cu and 18 Zn ions, and 1099 water molecules. The stereochemistry of the model was generally good. Ramachandran plots for the 18 monomers showed 86.0–92.6% of protein residues in the most favoured regions and 7.4–13.2% in additionally allowed regions. In four monomers (C, D, G and K), Asn26 was placed in the generously allowed region. The estimated standard uncertainty (ESU) implemented in REFMAC5[37] was 0.12 Å, which may be taken as the data-only positional uncertainty of an atom with a *B*-factor equivalent to that determined from a Wilson plot (26 Å^2). The rms deviations of bond lengths and angles from ideal values were 0.014 Å and 1.52°, respectively. The rms positional differences between dimers for main-chain atoms averaged over all nine dimers was 0.39 Å. A superposition of the α-carbon backbone atoms of all the dimers shows that the core of the structure, including the monomer–monomer interface, is constant, while there is greater flexibility in the loop regions

and at the N and C termini (Figure 1(a)). Omitting these regions from the calculation gives an average rms of 0.27 Å.

Superposition of the α-carbon backbone atoms of the nine dimers with the dimer of the published 2.5 Å resolution structure for wtSOD1[36] gave an average rms difference of 0.98 Å. There is considerable structural variation for the whole of the molecule, as shown in Figure 1(b), an observation we attribute mainly to the significantly improved resolution of the present structure. Similar differences in structure (average rms 0.78 Å) are apparent between the present wtSOD1 and the 2.4 Å structure of the thermostable double mutant Cys6Ala/Cys111Ser,[36] which was used as the parent structure for a recent study of the A4V FALS mutant (a C6A-C111S-A4V triple mutant in this case).[38] In Figure 1(c) a superposition is shown with the α-carbon backbone atoms of bovine SOD[9] (PDB code 1cbj), measured at a resolution (1.65 Å) comparable to the present wtSOD1 structure, the first human SOD structure determined at high resolution. The overall rms positional difference is 1 Å. However, the wtSOD1 amino acid sequence has a two residue insertion, Asn26 and Gly27, relative to the bovine sequence. This results in a significant positional deviation in the loop region in each monomer, from Lys23 to Pro28. When these residues are omitted from the calculation, the rms difference is 0.71 Å.

The wtSOD1 apo enzyme

The apo wtSOD1 model has been refined to an *R*-factor of 23.2% for all data in the resolution range 25–1.82 Å, with an R_{free} of 28.2% (Table 1). The protein crystallizes in space group *C*2 and the asymmetric unit contains four monomers or two dimers designated as A + B, C + D. The electron density allowed the positioning of 153 residues in subunits A and B with 90.1% of residues in the most favoured region of the Ramachandran plot and 9.9% in additionally allowed regions. The overall stereochemical *G*-factor was −0.01. Only 126 residues were placed in the electron density in subunits C and D, and the final model gave 88.9% of residues in the most favoured region of the Ramachandran plot, 11.1% in additionally allowed regions, and an overall stereochemical *G*-factor of −0.07. The stereochemical measures all fall within the inside or better limits set by the PROCHECK program, which compares the current model against a database of structures.[39] The final model from REFMAC5 gave rms deviations of bond lengths and angles from ideal values of 0.010 Å and 1.11°, respectively, with an ESU of 0.17 Å. The rms average positional difference for the main-chain atoms between dimer A + B and dimer C + D was 0.58 Å. A superposition of the α-carbon backbone atoms of the A + B dimer of apo wtSOD1 and the nine dimers of holo wtSOD1 gives an average rms positional difference of
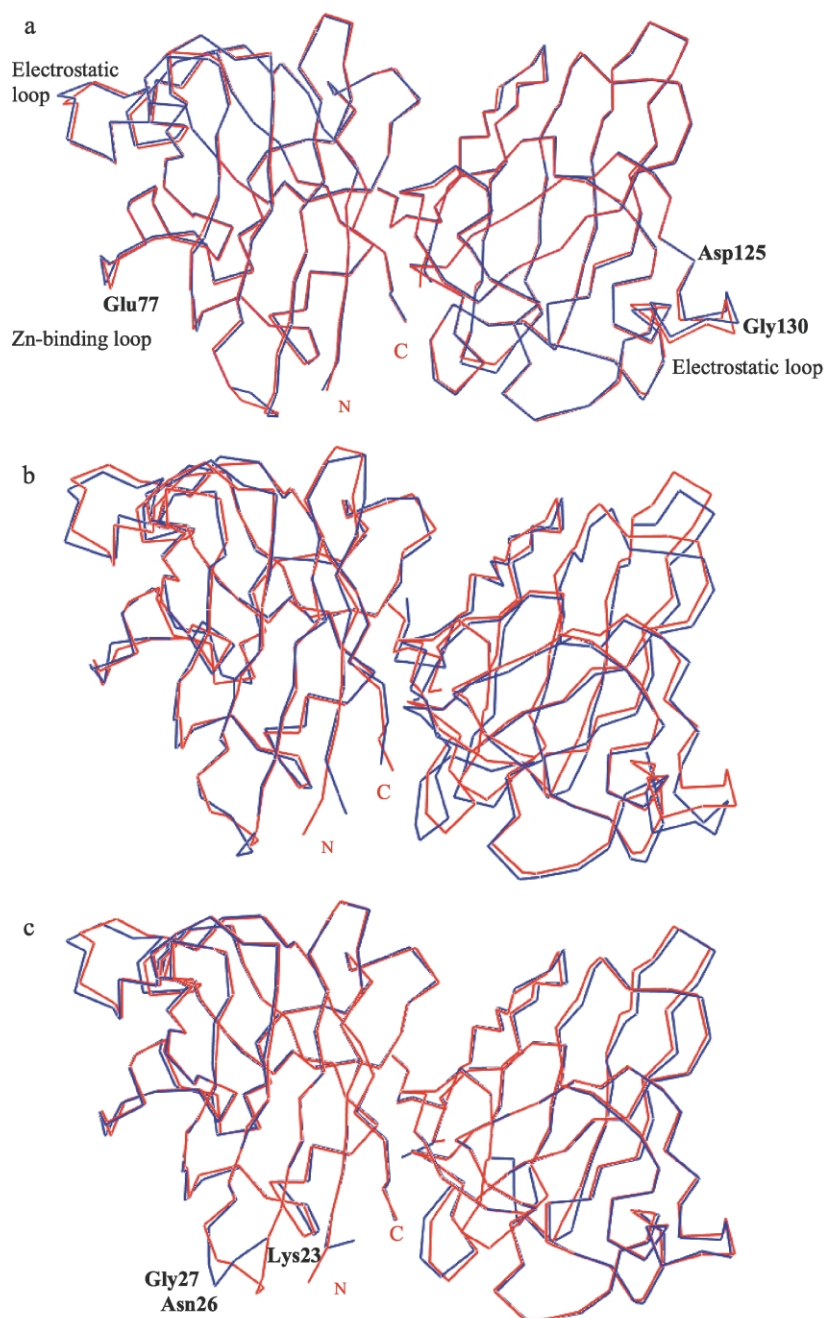
Figure 1. Superposition of the α-carbon backbone atoms of (a) the A + H (red) and G + N (blue) dimers of holo wtSOD1. The rms positional difference between them is 0.39 Å and is representative of the entire nine dimer model. The variation between the structures is most significant for the Zn-binding and electrostatic loop regions and the C and N terminii, while the monomer–monomer interface is relatively invariant; (b) holo wtSOD1 dimers from two crystal structures: the A + H dimer of the present 1.78 Å resolution data is shown in red; the dimer of the 2.5 Å resolution data[36] is shown in blue. The mean positional rmsd is 0.98 Å and variation between the two dimers is evident at the interface and metal-binding regions as well as the loop and terminii regions; (c) the A + H holo wtSOD1 dimer (red line) with the 1.65 Å resolution bovine SOD structure (blue line). The bovine data, measured at a comparable resolution to holo wtSOD1, provides a better model than the lower resolution wtSOD1 data. The two residue insertion in each wtSOD1 monomer compared to bovine SOD leads to disorder in the loop residues 23–28, as indicated in the Figure, and contributes 0.3 Å of the total 1 Å rmsd between the two dimers.

0.62 Å; for the C + D dimer the average rms is 0.74 Å. The final model contains 323 water molecules.

## The copper and zinc-binding sites

The wtSOD1 holo enzyme

The Cu ion is five co-ordinate in all dimers with a geometry described as distorted tetrahedral. Details of the metal ion coordination for all of the molecules in the asymmetric unit are given in Table 2. Cu forms bonds with His63, His48, His120 and His 46 at ∼2.1 Å. The Cu-His63-Zn imidazolate-bridge is intact, and electron density is present linking the Cu and Zn ions in all subunits (Figure 2, upper panel). Four strongly conserved water molecules, one of which is a Cu ligand, form a H-bonding network with each other and with residues Gly141 and Arg143 in the Cu site cavity (Figure 2, lower panel).

The Cu-His63 $N^{\varepsilon 2}$ separation varies from 2.3–2.8 Å, while the distance from Cu to the nearest water molecule lies between 2.4 Å and 3.1 Å. The separation of Cu and Zn varies between 6.35 Å and 6.55 Å. Previous structural studies[9,40] on Cu,Zn SODs from a range of sources, particularly the bovine enzyme, have indicated that a Cu−Zn separation of ∼6.0 Å and Cu-His63 $N^{\varepsilon 2}$ separation

Table 2. Comparison of bond distances (Å) and *B*-factors (Å²) at the metal sites of the nine dimers of wtSOD1

	A	H	B	I	C	J	D	K	E	L	F	M	G	N	O	Q	S	P
His48 NE2	2.14	2.11	2.11	2.12	2.11	2.09	2.08	2.12	2.09	2.05	2.10	2.12	2.14	2.06	2.19	2.06	2.02	2.11
His120 NE2	2.12	2.11	2.13	2.03	2.19	2.15	2.13	2.15	2.16	2.02	2.13	2.09	1.94	2.04	2.09	2.11	2.19	2.58
His46 ND1	2.14	2.13	2.12	2.12	2.13	2.15	2.18	2.11	2.15	2.08	2.04	2.11	2.04	2.12	2.15	2.09	2.18	2.04
His63 NE2	2.44	2.52	2.59	2.67	2.72	2.61	2.60	2.48	2.52	2.79	2.49	2.54	2.71	2.72	2.63	2.62	2.53	2.34
Wat1	2.62	2.72	2.46	2.88	2.51	2.63	2.64	2.65	2.71	3.11	2.74	2.62	2.5	2.40	2.5	2.73	–	–
CU *B*-factor	18.51	23.39	15.29	18.19	17.02	15.53	22.61	14.29	21.28	22.36	22.99	23.84	28.42	22.53	30.13	23.00	46.35	68.63
CU_ZN	6.37	6.43	6.48	6.46	6.46	6.42	6.47	6.37	6.42	6.55	6.41	6.35	6.43	6.42	6.43	6.37	6.36	6.08
Asp83 OD1	1.88	1.98	1.94	2.01	1.96	2.01	1.88	1.90	1.95	1.90	1.92	1.90	1.83	2.00	1.90	1.91	2.02	1.77
His71 ND1	1.99	2.05	2.00	2.06	2.05	2.07	2.06	2.13	2.00	2.06	2.08	2.05	2.10	1.97	1.95	2.03	2.11	2.10
His80 ND1	1.99	1.85	2.02	2.10	2.08	1.99	2.00	2.03	2.01	1.98	1.93	2.05	1.96	2.20	2.21	2.09	2.05	2.19
His63 ND1	2.03	2.02	1.99	1.95	1.94	1.95	2.02	1.97	2.02	2.01	2.03	1.96	2.12	1.97	2.03	1.93	2.08	2.15
Asp83 OD2	2.82	2.85	2.91	2.84	2.83	2.91	2.83	2.89	2.83	2.88	2.77	2.93	2.65	2.80	2.80	2.84	2.87	2.68
ZN *B*-factor	9.17	11.03	6.21	7.98	6.32	7.46	10.95	5.26	9.60	10.06	12.86	10.18	21.84	12.60	20.02	12.71	10.95	59.83
Overall *B* before TLS	30.4	30.3	25.8	26.2	25.2	25.7	30.4	25.0	29.3	31.5	34.8	30.0	44.2	34.3	43.5	35.5	39.4	50.2
Overall *B* after TLS	13.6	13.4	9.5	10.0	9.0	9.5	13.6	8.7	13.1	14.6	19.2	14.2	23.2	15.9	23.9	16.6	36.2	61.2
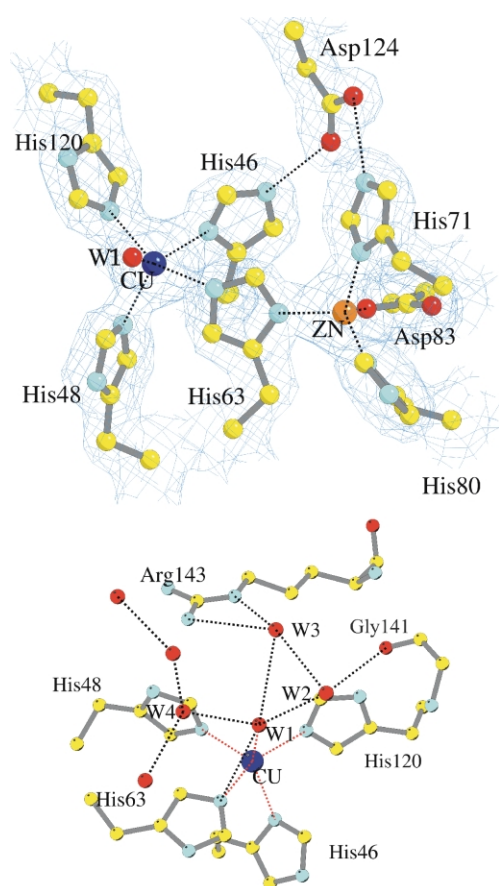
Figure 2. The $2F_o - F_c$ electron density map contoured at 1σ (upper panel) and water network (lower panel) of the Cu–Zn site of holo wtSOD1. Monomer A is shown here as representative of the active sites of all 18 monomers. The Cu atom possesses all four histidine ligands; the electron density map shows that the Cu-His63-Zn bridge is intact. A well ordered network of water molecules occupies the active-site channel. This is similar in all monomers, with slight differences in distances. The water molecule W1 is co-ordinated to Cu at a distance of ~2.6 Å. It also makes H-bonds to three further water molecules, W2, W3 and W4. Notably, only W3 in the active-site channel is in position to form a H-bond to the guanidine group of Arg143, linking the Arg143 residue and the metal-bound W1; there is no direct H-bonding between W1 and Arg143, the distance being ~4.2 Å. W1 is 2.7 Å from W2, which in turn has strong H-bonds to W3 at 2.8 Å and with the main-chain O atom of Gly141 at 2.9 Å. W1 has a weak H-bond with W3 at a distance of 3.3 Å, while W3 has a strong H-bond with the N^{ϵ} atom of Arg143 at 2.93 Å and a weaker H-bond with $N^{\eta 2}$ of Arg143 at 3.09 Å. The Cu-coordinated W1 also H-bonds to $N^{\delta 2}$ of His63 at ~3 Å.

of ~2.0 Å is indicative of Cu(II)-SOD, while in Cu(I)-SOD more typical separations would be Cu–Zn ~6.8 Å and Cu-His63 $N^{\epsilon 2} > 3.0$ Å. This results from a shift in the position of the Cu atom and a rotation of the ring of His63 out of the Cu–Zn plane upon reduction of the metal. The active sites in the wtSOD1 structure occupy conformations intermediate between that expected for

the oxidized and reduced forms of the enzyme. This may represent X-ray-induced photoreduction of Cu during data collection or may have occurred during the crystallization or cryo-protection processes. Rapid photoreduction is observed in solution samples of wtSOD1 exposed to X-rays at 100 K during X-ray absorption fine structure (XAFS) measurements (R.W.S. *et al*, unpublished results). It is possible that the steric and dynamic constraints imposed by the crystalline lattice limit the capability of the active site to adopt the three coordinate Cu geometry on reduction of the metal ion.[9]

The Zn ion is coordinated to Asp83 at ~1.9 Å, and to His71, His80 and His63 at ~2.0 Å. There is little variation in bond lengths between the sites in different monomers. The Zn sites in wtSOD1 are similar to those determined at lower resolution and in other Cu,Zn SODs, and are consistent with the results of XAFS data on human SOD1 (R.W.S. *et al*, unpublished results).

Substantial differences in the active-site coordination geometry exist between the present data and that provided by the earlier 2.5 Å resolution wtSOD1 crystal structure,[11] as shown in Figure 3(a). Consistent with the overall positional differences between these molecules, we suggest that the improved crystallographic resolution reported here is one reason for the observed differences. Evidence for this view is provided by Figure 3(b), where the present structure is compared to the Cu–Zn site in bovine SOD measured at 1.65 Å resolution,[9] which shows excellent agreement between their coordination environments.

The wtSOD1 apo enzyme

In the apo protein there is a clear difference between the active-site structures of the A + B and C + D dimers: while there is no metal at any of the Cu-binding sites or at the Zn-binding sites of the C and D monomers, there is evidence for residual metal binding at the Zn-binding site in subunits A and B. Zn atoms with occupancy 0.2 and B-factors 32 Å^2 and 38 Å^2, respectively, were therefore included at the Zn sites in monomers A and B in the final model. These values are consistent with the B-factors of the surrounding ligands. The Zn coordination is similar to that found for holo wtSOD1, with Asp83 in subunit A (B) at 2.04 Å (1.89 Å), His71 at 2.40 Å (2.16 Å), His80 at 1.94 Å (1.96 Å) and His63 at 2.10 Å (1.98 Å) (Figure 4(a)). For monomers A and B, the Cu and Zn-ligating residues and the surrounding Zn-binding and electrostatic loop regions are in conformations similar to those found in the wild-type.

Monomers C and D are both devoid of metals and the electrostatic and Zn-binding loops are disordered and not visible in the electron density maps. At the vacant Zn site, only His63 is seen clearly in the electron density maps (Figure 4(b)),

(a)

(b)
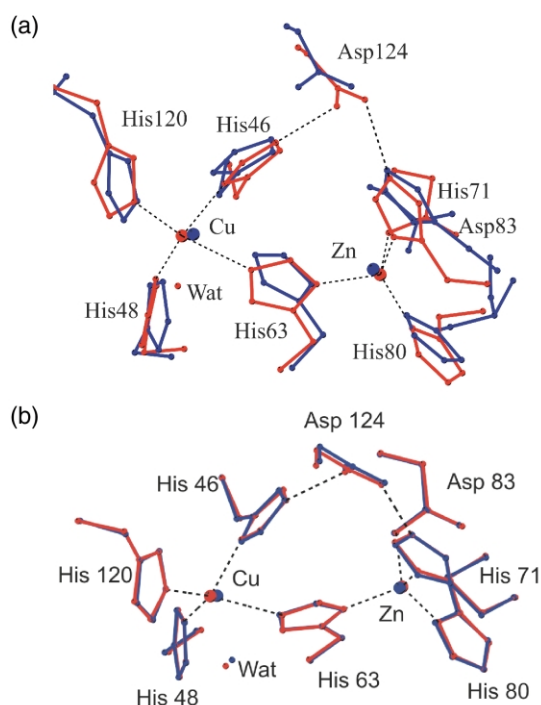
Figure 3. The active site of the 1.78 Å resolution holo wtSOD1 data reported here (shown by the red line) compared to (a) the Cu–Zn site of the 2.5 Å resolution holo wtSOD1 crystal structure (blue line). Superposition of the active sites using the other 17 monomers of the high-resolution structure gives identical results. The differences between the two wtSOD1 coordination geometries is likely to be due to the different resolution limits of the two datasets. This is suggested by (b) a comparison with the Cu–Zn site of the 1.65 Å resolution crystal structure of metallated bovine SOD (red line), with the oxidised (blue line) Cu centre. The agreement between the active-site structures is clearly better for the higher-resolution bovine data.

where its position is close to that in the native structure. The remaining residues that usually form this site are disordered: His71 is absent altogether and only the main-chain of His80 is visible; in monomer C, Asp83 is rotated to form a bond with Asp124, replacing the H-bond normally made by His71. However, the electron density for the Asp83 side-chain is weak and the $O^{\delta1}$ and $O^{\delta2}$ atoms have only 0.5 occupancy. In monomer D, the Asp83 side-chain is not visible in the electron density.

The four histidine residues that normally ligate Cu are clearly visible in the electron density in both monomers: His48 and His120 are shifted slightly from their position in the native structure and the largest movement is made by His46, which is rotated by ~120° about the C^{β}–C^{γ} vector compared to its orientation in the native protein. The H-bond from His46 to Asp124 is retained in this structure due to an approximate 90° rotation of the Asp124 side-chain towards the histidine residue (Figure 4(c)).

## Disordered loop regions and metal binding in apo wtSOD1

The orientation of the two dimers in the asymmetric unit and the arrangement of their electrostatic (residues 125–140) and Zn-binding (residues 67/68–78) loops are illustrated by Figure 5. The C and D monomers are completely devoid of metals and are significantly disordered in these loop regions, which cannot be seen in the electron density maps. In both monomers, the secondary bridge H-bonding network is disrupted and His71 is completely disordered. The electrostatic loop region (from residue 125 onwards) is disrupted, with the side-chain of Asp124 no longer able to form a contact with Leu126 and is instead rotated to point towards the Cu site. In monomer C, the Asp83 residue is rotated to form a weak bond with Asp124 (the Asp83 side-chain is too disordered to observe this in monomer D). The Cu-ligating residues remain largely unchanged, except for His46, which moves significantly to remain in contact with the reoriented Asp124. The lack of metal in this dimer is therefore associated with major disturbances in the structure that extend well beyond the Cu and Zn-binding sites.

These observations tend to support the view[23] that His71, together with the H-bonding network involving the Cu-ligating His46, Asp124 and the Zn-ligating His71, are crucial elements in forming a correctly oriented Zn-binding site and in the stabilization of the Zn-binding and electrostatic loops. The structure is consistent with a solution NMR study of a monomeric Cu,Zn SOD1 that suggested that the H-bonding arrangements centred around Asp124 have a significance for Zn affinity and that Asp124 might act as a determinant for Zn binding.[41]

Metal deficiency may not be the sole cause of the loop disorder. The A and B monomers also lack Cu and have only ~20% occupancy at the Zn site, yet they possess well ordered Zn-binding and electrostatic loop regions. These correspond closely to the arrangement found in the wild-type holo protein, with His71 and the His46-Asp124-His71 secondary bridge intact, and with Asp124 forming a H-bond with Leu126. Since these data show that the ~80% metal-deficient A + B dimers have fully ordered loop regions, this feature of the crystal structure must involve factors in addition to metallation at the Zn site, such as the crystal packing forces. This view is supported by crystallographic studies on the SOD1 FALS mutant apo-H46R.[35]

Crystal packing in holo and apo wild-type SOD1

The packing of molecules in the *P*21 crystal form of wtSOD1 reported here shares a common factor with that of the previously published *C*2221 crystal form:[36] the presence of a 'trimer of dimers' in their respective asymmetric units (Figure 6). We have
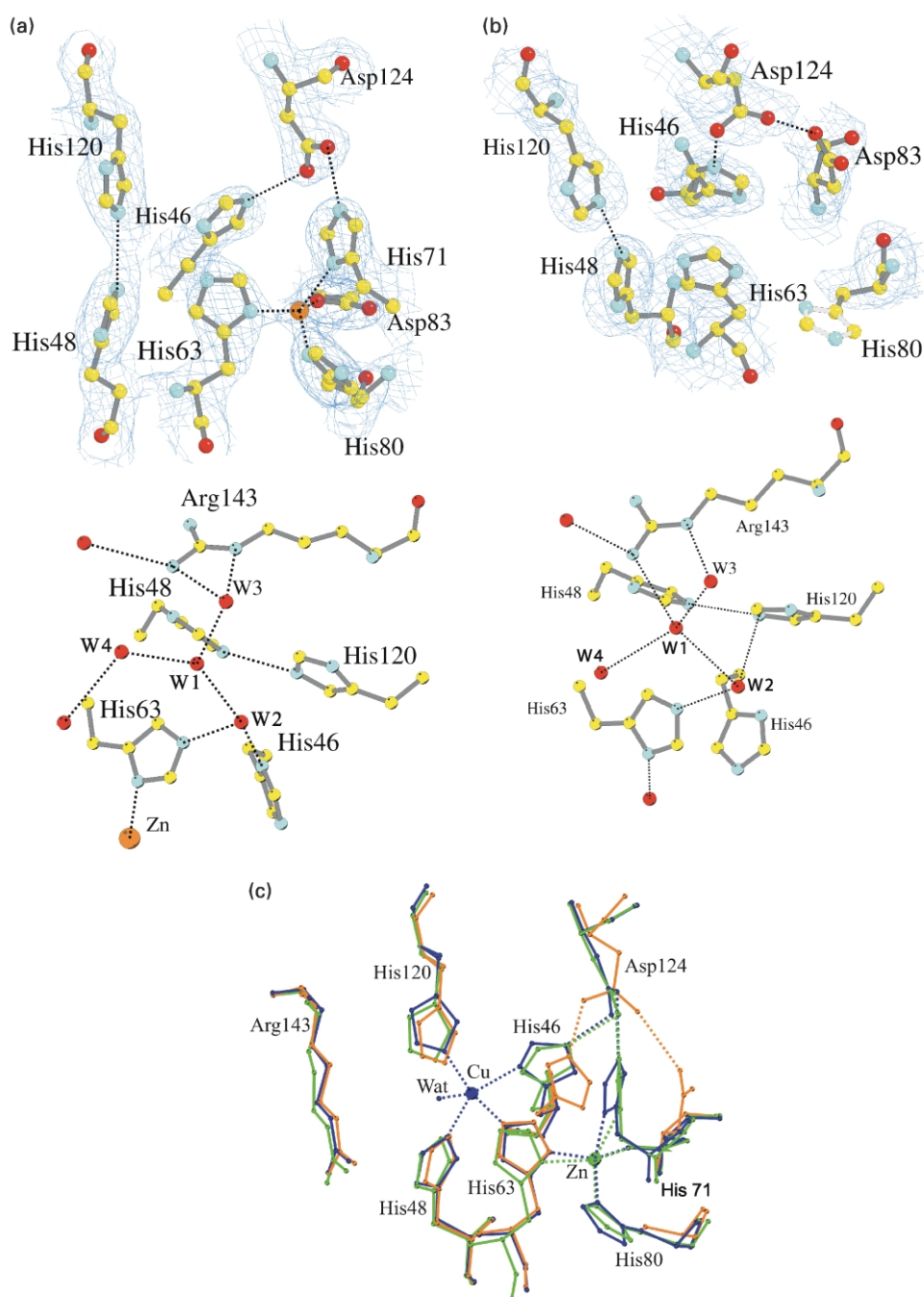
Figure 4. The $2F_o - F_c$ electron density maps (contoured at 1σ) and the water networks at the metal-binding sites of apo wtSOD1: (a) monomer A, showing partial Zn occupancy and a Zn-binding loop in a conformation similar to that of the wild-type protein. All the Zn ligands are visible in the electron density and the His46-Asp124-His71 secondary bridge is intact. (b) Monomer C, where the Zn-binding loop is disordered and significant rearrangement of the H-bonding network involving His46, Asp124 and Asp83 has occurred. Asp83 has rotated to form a contact with Asp124 in the absence of the His71 residue, which is not seen in the electron density. The imidazole ring of His80 is shown for visual reference but does not have any corresponding electron density. The water network at the metal-binding site of the apo enzyme is different from that of the holo enzyme (see lower panels and Figure 2). There are some differences between the water structure in the two disordered monomers. The only strictly conserved water molecule is W3, which is the lone water molecule present at the Cu-binding site of monomer D (not shown). A group of four water molecules (W1–W4) is present in monomers A, B and C but they interact with the protein residues some-what differently. In monomers A and B, W3 has two H-bonds with Arg143, identical with the holo enzyme, and a third H-bond with W1. His63 and His46 participate in the H-bonding water network, interacting with W2, whereas Gly141 is no longer involved. In monomer C, W2 interacts with W1 and protein residues His63 and His120, but His46 is no longer in position to interact with this water molecule. Interestingly, the partial occupancy Zn atom present in monomers A and B is replaced by a full occupancy water molecule in monomer C, which forms a H-bond with His63. (c) Comparison of the holo wtSOD1 metal-binding site of monomer A (blue) with those for apo wtSOD1
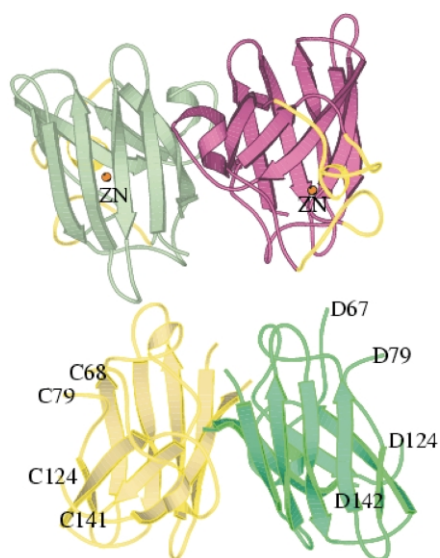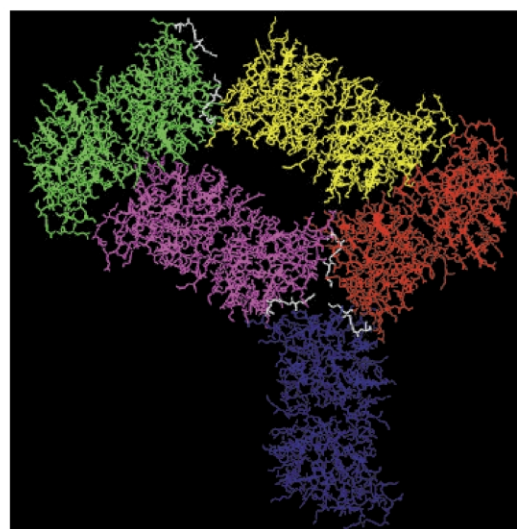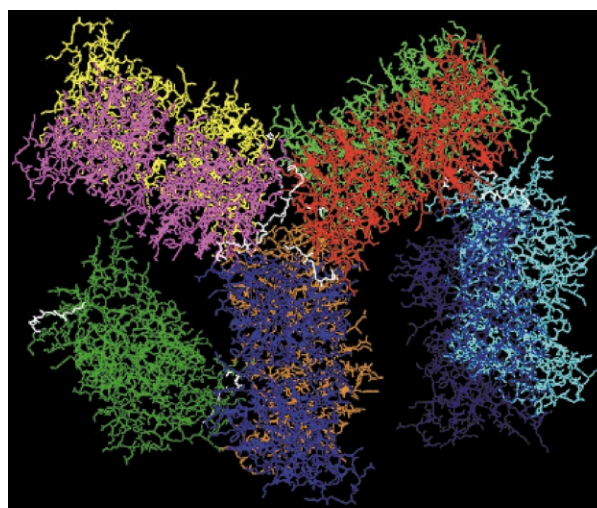
Figure 5. The arrangement of the two dimers in the asymmetric unit of apo wtSOD1. The positions of the disordered Zn-binding (residues 67/68–78) and electrostatic (residues 125–141) loops are indicated.

observed variations of this packing arrangement in the metallated crystal structures of the FALS-related SOD1 mutants A4V, L38V and H43R (S.A. *et al.*, unpublished results), and here we describe our own unpublished data for the *C*2221 crystal form of wtSOD1. In the *P*21 crystal form, two such trimers are stacked along the short crystallographic *a* axis and the addition of three more dimers completes the asymmetric unit (Figure 6, upper panel). In the *C*2221 crystal form, a single trimer of dimers in the asymmetric unit is accompanied by two dimers that form part of a second trimer (Figure 6, lower panel); in this structure, stacking occurs along the shortest crystallographic axis, the *c* axis. The head-to-head interactions at the trimeric interface involve the electrostatic loop residues 128–131, shown in white in Figure 6. H-bonding between this loop region of the interfacing monomer and the Thr88, Asp96 and Ser98 (NB all in the Zn-loop) residues of a second monomer form the main contacts. Thr88 and Ser98 are involved in H-bonding with the electrostatic loop at the dimer–dimer interface of the apo protein.

Diagrams to illustrate the molecular packing of the apo enzyme are shown in Figure 7. Viewed along the crystallographic *b* axis (Figure 7(a)), the A + B and C + D dimers form a two-dimensional array of β-barrels. The tetramer A + B + C + D comprising the asymmetric unit is surrounded by

Figure 6. The arrangement of the nine dimers in the asymmetric unit of P21 holo wtSOD1 (upper panel) and the five dimers in the asymmetic unit of C2221 wtSOD1 (lower panel; our own unpublished data, similar to that described by Parge *et al.*[36] for this crystal form). The dimers are coloured differently as an aid to viewing. The trimer of dimers motif is evident. The electrostatic loop residues (128–131) involved in H-bonding interactions at the trimeric interfaces are highlighted in white.

four others in the *ac* plane. This results in alternate rows of head-to-head packing of dimers with the sequences (A-B)–(C1-D1) and (D-C)–(B2-A2). The contacts at the monomer–monomer interfaces, A to B and C to D, are identical and involve H-bonding from Gly51 and Gly114 of one molecule to Ile151 of the other. The intermolecular contacts between the two dimers in the asymmetric unit

monomers A (green) and C (orange). The Zn and Cu-binding residues in monomer A of the apo protein and in the holo protein are oriented similarly but there is a significant shift in orientation for the same residues in monomer C at the Cu site, while the bridging His63 ligand and His48 are relatively unchanged. At the Zn site, both His80 and His71 are "missing" from the structure in monomer C.
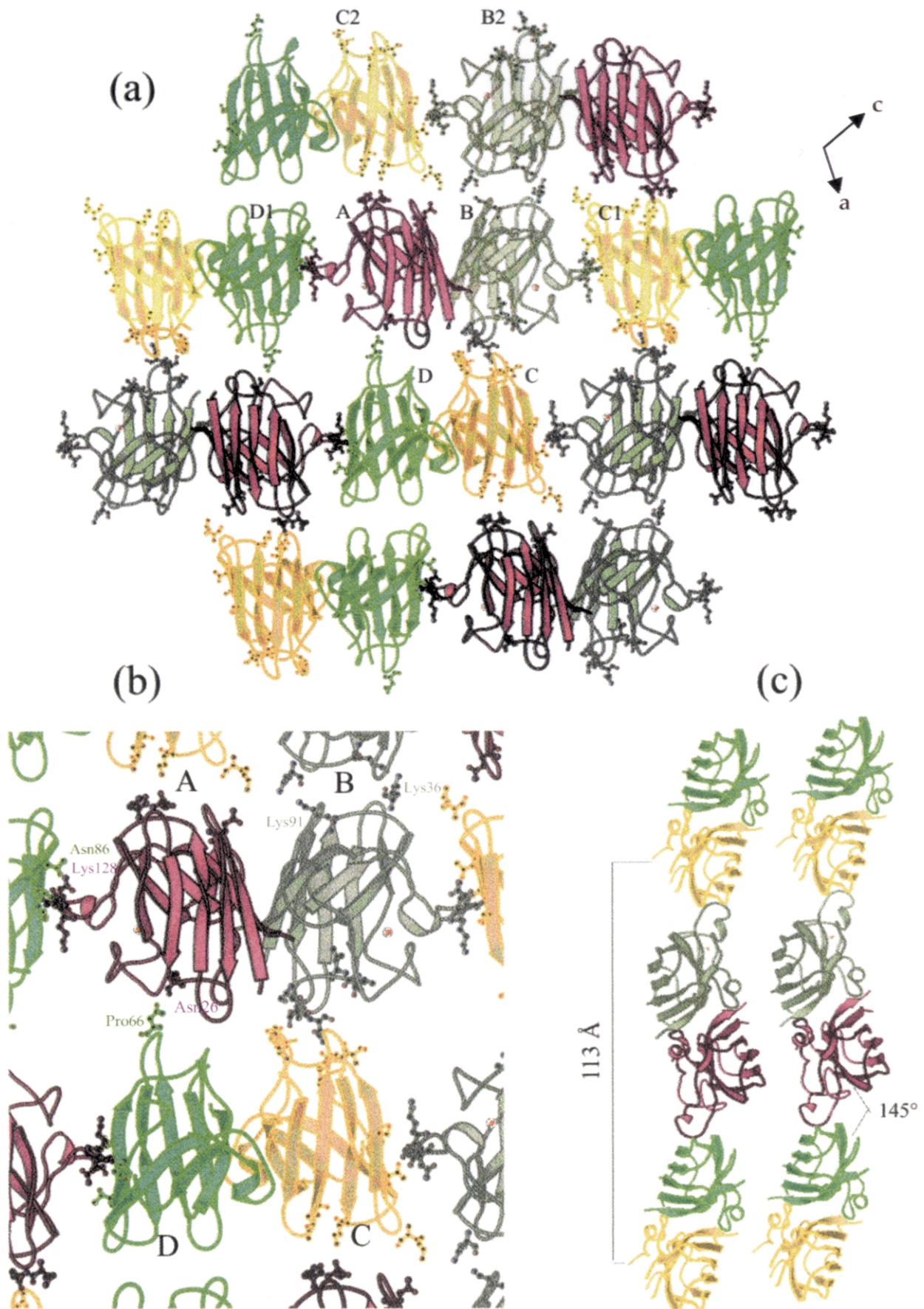
Figure 7. Packing of molecules in apo wtSOD1. (a) The apo-protein has an extended sheet of β-barrels arranged in the ac plane. Monomer A is shown in red, B in light green, C in yellow, D in green. Adjacent, identical monomers are

are between monomers A and D, and monomers B and C. The H-bonding connections are different in the two cases and are illustrated in detail in Figure 7(b).

A further set of contacts exist in the head-to-head packing arrangement between dimer A + B and adjacent monomers C1 + D1 (see Figure 7(b)). This arrangement involves H-bonding between the electrostatic loop region (residues Lys128-Asn131) of the intact monomers A and B, and the residues (Asn86, Thr88 and Ser98) that lie between the disordered electrostatic and Zn-binding regions of monomers D1 and C1, respectively.

Two B monomers of adjacent tetramers (B and B2 in Figure 7(a)) are linked by a strong H-bond between lysine residues, the NZ atom of Lys36 and the O atom of Lys91. Monomers A and C2 of two different tetramers are linked by two strong (Lys91 O with Gln15 NE2 and Asp92 O with Lys36 NZ) and one weak (Gln15 NE2 to Lys91 O) H-bond.

The view parallel with the crystallographic *a*-axis (Figure 7(c)) shows that the β-barrel array is not linear, but zig-zags in and out of the *ac* plane with a repeat length of 113 Å. The angular deviation from linear orientation, measured at the dimer–dimer interface, is ~145°. The head-to-head packing of the dimers forms a set of parallel β-sheets running perpendicular to the long (*a* to *c*) diagonal of the unit cell. The closest approach between adjacent sheets is ~6 Å (Glu49 to Lys30).

The Asn86 residue in monomers C + D participates in four strong H-bonds at the dimer–dimer interface, to residues Lys128-Gly130 of the ordered monomers A and B. This residue is not involved in H-bonding in the wild-type protein. The closest approach of Asn86 to Lys128 across the trimeric interface of wtSOD1 is ~10 Å, compared to 2.9 Å in the apo protein. It appears that the disorder in the electrostatic loop region of one pair of dimers in the apo protein allows a deeper penetration of the head-to-head packing of the apo dimers, forming a more obtuse angle between them, ~145° compared to 120° in wild-type. Thus, the trimer of dimers building block that is present in the metallated wild-type protein is disrupted in the apo protein due to loss of metal or to loop disorder (or

both). A similar packing motif appears in the crystal structure of the apo-H46R FALS mutant of SOD1,[35] where the asymmetric unit consists of three dimers with disorder in the Zn and electrostatic loop regions and one dimer with intact loops. This results in two types of head-to-head packing of the dimers. The same zig-zag motif that is present in the apo wtSOD1 structure occurs in apo-H46R when one "intact" and one "disordered" dimer interact. In addition, a fully linear head-to-head packing arrangement is seen in the structure when both of the interacting dimers possess disordered Zn and electrostatic loops. There is therefore a progression in the head-to-head packing geometry in the SOD1 crystal structures, from the 120° trimer of dimers, with each (metallated) dimer possessing fully ordered loop regions, to the 145° zig-zag arrangement with disordered loops in one of the dimers, to the linear arrangement of dimers where both possess disordered loops.

The molecular packing present in the apo wtSOD1 structure and in the crystallographically characterized FALS SOD1 mutants H46R and S134N[35] is highly significant, in that it resembles a structure that is common to the formation of amyloid-like fibrils found in a range of neurodegenerative diseases including Creutzfeld–Jakob disease and Alzheimer's disease. X-ray fibre diffraction studies have shown that there exists a generic β-sheet amyloid fibril structure regardless of the native fold of the amyloidogenic protein: this structure, determined from six different *ex vivo* and two synthetic amyloid fibrils, has a helical repeat of 115.5 Å containing 24 β-strands.[42] This compares with a helical repeat of 113 Å for apo SOD1. Formation of the fibril structure from the native protein fold requires significant conformational change for proteins with extensive α-helical content, as observed for example in scrapie prion proteins.[43] Being composed primarily of β-sheets, Cu,Zn SOD1 is well suited for performing the necessary structural conversion. Indeed, the comparison with the wild-type protein suggests that the interaction between the SOD1 dimers can be altered by the loss of Zn and perhaps Cu, and the accompanying loss of order in the Zn-binding and electrostatic loop regions. The

labelled A1, B1 etc; (b) contacts between neighbouring dimers in the asymmetric unit: H-bonds involving OD1 and ND1 of Asn26 and the O atom of Pro66 are symmetrically involved in interactions between A and D. Asn26 is a key residue in the H-bonding between monomers B and C, where the ND1 nitrogen atom is linked with the O atoms of Val103, Ile104 and (a weaker H-bond) Ser102. In addition, there is a H-bond between the OE2 atom of Glu24 and the OD2 atom of Asp109 and a weaker H-bond between Ser25 OG and the O atom of Ser107. The H-bonding network involving molecules in adjacent asymmetric units: between monomers A and D1 there are seven strong and three weak H-bonds. The O atom of Lys128 in monomer A forms H-bonds with the N, O (strong) and ND2 (weak) atoms of Asn86 of monomer D1. The O atom of Gly129 has H-bonds to the O atom of Asn86 and to the N (weak) and OG1 (strong) atoms of Thr88. The N and O atoms of Gly130 participate in three H-bonds: to Asn86 O and to Ser98 N and O atoms, respectively. Finally, the N atom of Asn131 forms a weak H-bond to the O atom of Ser98. H-bonding network B to C1: the H-bond lengths are longer in most cases and there are six strong and two weak interactions; (c) the view obtained after rotating figure (a) twice by 90° showing the "zig-zag" arrangement of the constituent β-strands aligned along the long *ac* diagonal of the unit cell.

trimer of dimers present in the wild-type protein is then replaced by a dimer of dimers building block, whose repeat motif results in the extended two-dimensional arrays of stacked β-sheets observed in the apo structure, as well as in the metal-depleted S134N and apo-H46R FALS mutants.[35]

The importance of the apo form of the protein may explain why the ~ 100 diverse point mutations of SOD1 can all result in toxic gain of function: these mutations may induce a more labile Zn-binding and a less stable protein than the wild-type metallated protein. A recent study has shown that a common factor in the ALS mutants appears to be the decreased stability of the demetallated forms of the proteins,[44] with the less stable mutants resulting in shorter survival times for patients. Intriguingly, SOD1 enters the inter-membrane space of mitrochondria as the apo protein.[34] Failure to incorporate metal could result in the long-term accumulation of the apo protein.

Conclusions

The first high-resolution crystal structures of fully metallated wild-type human Cu,Zn superoxide dismutase and a metal-deficient wild-type apo enzyme have been determined. These structures have a direct relevance to our understanding of the causes of familial amyotrophic lateral sclerosis, a disease in which mutations of the SOD1 gene have been implicated. The structure of the apo enzyme has revealed that the normal homodimeric building block can exist with two forms of dimer: one in which the Zn site is partially occupied and the Zn-binding and electrostatic loops are well ordered; and a second dimer, which is completely de-metallated and possesses disordered loop regions. The loss of order in these loops allows a closer than normal head-to-head interaction between the β-strands of adjacent dimers, resulting in an extended β-sheet structure resembling that found in structures associated with neurodegenerative diseases.

Materials and Methods

Crystallization and data collection

Recombinant human SOD protein was expressed and purified as described.[22] Crystals of wtSOD1 were grown using the hanging-drop, vapour-diffusion technique. Droplets containing a concentration of 6 mg/ml of protein with 7.5% (w/v) PEG 3350, 100 mM calcium acetate, 50 mM Tris (pH 8.0) were equilibrated over wells containing 15% PEG 3350, 200 mM calcium acetate, 100 mM Tris–HCl (pH 8.0). Crystals grew in four to seven days up to 1.5 mm in length. Data were collected at 100 K using an ADSC Quantum 4 CCD detector on the 2 T multipole wiggler beam line 14.2 at the Daresbury Synchrotron Radiation Source using a wavelength of 0.978 Å to a resolution limit of 1.78 Å. Data were pro-

cessed using HKL2000.[45] A total of 265,996 unique reflections were obtained with an R_{merge} of 5.2%. The crystals were found to be of space group $P21$ with unit cell parameters of $a = 76.8$ Å, $b = 172.3$ Å, $c = 112.5$ Å, $\alpha = \gamma = 90°$, $\beta = 93.5°$.

For crystallization of apo wtSOD1, droplets containing 6 mg/ml protein with 10% PEG2000, 100 mM ammonium chloride, 50 mM Mes (pH 5.6), equilibrated over wells containing 20% PEG 2000, 200 mM ammonium chloride, 100 mM Mes buffer (pH 5.6). Thick plates grow in four to seven days up to 0.2 mm × 1.0 mm × 0.05 mm. Data for the apo protein in space group $C2$ were collected at 100 K using the multipole wiggler beam line 14.2, to a resolution of 1.82 Å. After processing with program HKL2000 a total of 50,360 unique reflections were obtained with an R-merge of 6.1% respectively on equivalent intensities. Data collection statistics and cell parameters are summarised in Table 1.

Structure solution and refinement

The wtSOD1 holo enzyme

The structure was solved by the molecular replacement method using the program MOLREP.[46] A dimer of the 2.5 Å resolution structure[36] (PDB code 1sos) of the wtSOD1 double mutant (C6S, C111S) was used as a starting model.

The rotation function solution gave nine peaks from 7.5 σ to 4.5 σ, which corresponded to the presence of nine dimers in the crystallographic asymmetric unit. The translation function allowed the positioning of six dimers with a correlation coefficient (CC) of 0.49 and R-factor 38%. Initial refinement of this partial model was carried out without NCS restraints, using the maximum likelihood method as implemented in REFMAC5.[37] The use of this improved model allowed three additional dimers to be located by further application of the MOLREP program. The complete model of nine dimers gave a CC of 0.75 and R-factor 26.2%. Model building was carried out using O.[47] Maximum likelihood positional refinement, individual atomic B-factor refinement and overall anisotropic scaling were used. Solvent molecules were added using ARP.[48] The water molecules were gradually added to the model and were positioned only when well-defined positive peaks were present in both $2F_o - F_c$ and $F_o - F_c$ electron density maps and when they could form H-bond(s) with either protein atoms or other water molecules. A total of 800 water molecules were included in the final model.

The average isotropic temperature factors for the 18 wtSOD subunits (A, B, C, D, E, F, G, O, S, H, I, J, K, L, M, N and Q) present in the asymmetric unit were 30.4, 25.8, 25.2, 30.2, 29.3, 34.8, 44.3, 43.5, 50.3, 30.4, 26.2, 25.7, 31.5, 30.1, 34.3, 35.5 and 39.4 Å², respectively. This shows different overall thermal displacement parameters for the molecules in the asymmetric unit. To describe the translation, libration and screw-rotation displacement of each monomer modelled as a pseudo-rigid body, we used TLS refinement.[49] Initially, the B-factors of individual atoms were fixed to 20 Å² and were refined in the later stages of refinement. Each monomer was treated as a single TLS group and water molecules were excluded. This step in the refinement gave a drop in R-factor of 2.3% and in R_{free} of 2.1%, converging to a final R-factor of 18.5% and an R_{free} of 22.2% (Table 1).

The wtSOD1 apo enzyme

The structure was solved by molecular replacement using AMoRe.[50] A dimer of the 2.5 Å resolution structure of the SOD1 double mutant[36] was used as the search model. The top solution gave a tetramer in the asymmetric unit with *CC* of 59.7 and *R*-factor of 44.5% following rigid-body refinement. Further refinement of the model was performed along the same lines as with the holo wtSOD1 data, using REFMAC5 and ARP and with manual rebuilding using O. TLS refinement was used for the apo data and improved the *R*-factor and R_{free} by 0.6% and 1.7%, respectively. Refinement converged to a final *R*-factor of 23.2% and R_{free} of 28.2%. The mean *B* value fell from 46 Å² before TLS to 27.5 Å² afterwards. A summary of the structure refinement is given in Table 1.

Protein Data Bank accession codes

The final coordinates for both structures have been deposited in the Brookhaven Protein Data Bank (ID codes: 1HL5 (wtSOD1) and 1HL4 (apo)).

References

1. Fridovich, I. (1975). Superoxide dismutase. *Annu. Rev. Biochem.* **44**, 147–159.
2. Tainer, J. A., Getzoff, E. D., Beem, K. M., Richardson, J. S. & Richardson, D. C. (1982). Determination and analysis of the 2 Å structure of copper, zinc superoxide dismutase. *J. Mol. Biol.* **160**, 181–217.
3. Getzoff, E. D., Tainer, J. A., Weiner, P. K., Kollman, P. A., Richardson, J. S. & Richardson, D. C. (1983). Electrostatic recognition between superoxide and copper, zinc superoxide dismutase. *Nature*, **306**, 287–290.
4. Blackburn, N. J., Hasnain, S. S., Binsted, N., Diakun, G. P., Garner, C. D. & Knowles, P. F. (1984). An extended X-ray absorption fine structure study of bovine erythrocyte superoxide dismutase in aqueous solution. *Biochem. J.* **219**, 985–990.
5. Ogihara, N., Parge, H. E., Hart, P. J., Weiss, M. S., Goto, J. J., Crane, B. R. *et al.* (1996). Unusual trigonal-planar configuration revealed in the atomic structure of yeast copper–zinc superoxide dismutase. *Biochemistry*, **35**, 2316–2321.
6. Murphy, L. M., Strange, R. W. & Hasnain, S. S. (1997). A critical assessment of the evidence from XAFS and crystallography for the breakage of the imidazolate bridge during catalysis in CuZn superoxide dismutase. *Structure*, **5**, 371–379.
7. Ascone, I., Castamer, R., Bolognesi, M., Tarricone, C., Strappolo, M. E. & Desideri, A. (1997). Evidence of His61 imidazole bridge rupture in reduced crystalline Cu,Zn superoxide dismutase. *Biochem. Biophys. Res. Commun.* **241**, 119–121.
8. Hart, P. J., Liu, H., Pellegrini, M., Nersissian, A. M., Gralla, E. B., Valentine, J. S. & Eisenberg, D. (1998). Subunit asymmetry in the three dimensional structure of a human CuZnSOD mutant found in amyotrophic lateral sclerosis. *Protein Sci.* **7**, 545–555.
9. Hough, M. & Hasnain, S. S. (1999). Crystallographic structures of bovine copper–zinc superoxide dismutase reveal asymmetry in two subunits: functionally important three and five coordinate copper sites captured in the same crystal. *J. Mol. Biol.* **287**, 579–592.
10. Rosen, D. R., Siddique, T., Patterson, D., Figlewicz, D. A., Sapp, P., Hentati, A. *et al.* (1993). Mutations in Cu/Zn superoxide-dismutase gene are associated with familial amyotrophic-lateral-sclerosis. *Nature*, **362**, 59–62.
11. Deng, H.-X., Hentati, A., Tainer, J. A., Iqbal, Z., Cayabyab, A., Hung, W. Y. *et al.* (1993). Amyotrophic-lateral-sclerosis and structural defects in Cu,Zn superoxide-dismutase. *Science*, **261**, 1047–1051.
12. Borchelt, D. R., Lee, M. K., Slunt, H. S., Guarnieri, M., Xu, Z. S., Wong, P. C. *et al.* (1994). Superoxide-dismutase-1 with mutations linked to familial amyotrophic-lateral-sclerosis possesses significant activity. *Proc. Natl Acad. Sci. USA*, **91**, 8292–8296.
13. Bowling, A. C., Barkowski, E. E., McKennayasek, D., Sapp, P., Horvitz, H. R., Beal, M. F. & Brown, R. H. (1995). Superoxide-dismutase concentration and activity in familial amyotrophic-lateral-sclerosis. *J. Neurochem.* **64**, 2366–2369.
14. Gurney, M. E., Pu, H., Chiu, A. Y., Dal Canto, M. C., Polchow, C. Y., Alexander, D. D. *et al.* (1994). Motor neuron degeneration in mice that express a human Cu, Zn superoxide dismutase mutation. *Science*, **264**, 1772–1774.
15. Nishida, C. R., Gralla, E. B. & Valentine, J. S. (1994). Characterisation of three yeast copper–zinc superoxide dismutase mutants analagous to those coded for in familial amyotrophic lateral sclerosis. *Proc. Natl Acad. Sci. USA*, **91**, 9906–9910.
16. Rabizadeh, S., Grall, E. B., Borchelt, D. R., Gwinn, R., Valentine, J. S., Sisodia, S. *et al.* (1995). Mutations associated with amytrophic lateral sclerosis convert superoxide dismutase from an antiapoptotic gene to a proaptoptic gene: studies in yeast and neural cells. *Proc. Natl Acad. Sci. USA*, **92**, 3024–3028.
17. Wiedau-Pazos, M., Goto, J. J., Rabizadeh, S., Gralla, E. B., Roe, J. A., Lee, M. K. *et al.* (1996). Altered reactivity of superoxide dismutase in familial amyotrophic lateral sclerosis. *Science*, **271**, 515–518.
18. Yim, M. B., Kang, J. H., Yim, H. S., Kwak, H. S., Chock, P. B. & Stadtman, E. R. (1996). A gain-of-function of an amyotrophic lateral sclerosis-associated Cu,Zn-superoxide dismutase mutant: an enhancement of free radical formation due to a decrease in K-m for hydrogen peroxide. *Proc. Natl Acad. Sci. USA*, **93**, 5709–5714.
19. Cleveland, D. W. & Rothstein, J. D. (2001). From Charcot to Lou Gehrig: Deciphering selective motor

neuron death in ALS. *Nature Rev. Neurosci.* **2**, 806–819.

20. Crow, J. P., Sampson, J. B., Zhuang, Y. X., Thompson, J. A. & Beckman, J. S. (1997). Decreased zinc affinity of amyotrophic lateral sclerosis-associated superoxide dismutase mutants leads to enhanced catalysis of tyrosine nitration by peroxynitrite. *J. Neurochem.* **69**, 1936–1944.

21. Lyons, T. J., Liu, H., Goto, J. J., Nersissian, A., Roe, J. A., Graden, J. A. *et al.* (1996). Mutations in copper–zinc superoxide dismutase that cause amytrophic lateral sclerosis alter the zinc binding site and the redox behavior of the protein. *Proc. Natl Acad. Sci. USA*, **93**, 12240–12244.

22. Hayward, L. J., Rodriguez, J. A., Kim, J. W., Tiwari, A., Goto, J. J., Cabelli, D. E. *et al.* (2002). Decreased metallation and activity in subsets of mutant superoxide dismutases associated with familial amyotrophic lateral sclerosis. *J. Biol. Chem.* **277**, 15923–15931.

23. Lyons, T. J., Nersissian, A., Huang, H., Yeom, H., Nishida, C. R., Graden, J. A. *et al.* (2000). The metal binding properties of the zinc site of yeast copper–zinc superoxide dismutase: implications for amytrophic lateral sclerosis. *J. Biol. Inorg. Chem.* **5**, 189–203.

24. Beckman, J. S., Estevez, A. G. & Crow, J. R. (2001). Superoxide dismutase and the death of motoneurons in ALS. *Trends Neurosci.* **24**, S15–S20.

25. Crow, J. P., Ye, Y. Z., Strong, M., Kirk, M., Barnes, S. & Beckman, J. S. (1997). Superoxide dismutase catalyzes nitration of tyrosines by peroxynitrite in the rod and head domains of neurofilament-L. *J. Neurochem.* **69**, 1945–1953.

26. Estevez, A. G., Crow, J. P., Sampson, J. B., Reiter, C., Zhuang, Y. X., Richardson, G. J. *et al.* (1999). Induction of nitric oxide-dependent apoptosis in motor neurons by zinc-deficient superoxide dismutase. *Science*, **286**, 2498–2500.

27. Bruijn, L. I., Houseweart, M. K., Kato, S., Anderson, K. L., Anderson, S. D., Ohama, E. *et al.* (1998). Aggregation and motor neuron toxicity of an ALS-linked SOD1 mutant independent from wild-type SOD1. *Science*, **281**, 1851–1854.

28. Watanabe, M., Dykes-Hoberg, M., Culotta, V. C., Price, D. L., Wong, P. C. & Rothstein, J. D. (2001). Histological evidence of protein aggregation in mutant SOD1 transgenic mice and in amyotrophic lateral sclerosis neural tissues. *Neurobiol. Dis.* **8**, 933–941.

29. Wang, J., Xu, G. & Borchelt, D. R. (2002). High molecular weight complexes of mutant superoxide dismutase 1: age-dependent and tissue-specific accumulation. *Neurobiol. Dis.* **9**, 139–148.

30. Durham, H. D., Roy, J., Dong, L. & Figlewicz, D. A. (1997). Aggregation of mutant Cu/Zn superoxide dismutase proteins in a culture model of ALS. *J. Neuropath. Expt. Neurol.* **56**, 523–530.

31. Bredesen, D. E., Ellerby, L. M., Hart, P. J., Wiedau-Pazos, M. & Valentine, J. S. (1997). Do post-translational modifications of CuZnSOD lead to sporadic amyotrophic lateral sclerosis? *Ann. Neurol.* **42**, 135–137.

32. Jaarsma, D., Rognoni, F., van Duijn, W., Verspaget, H. W., Haasdijk, E. D. & Holstege, J. C. (2001). CuZn superoxide dismutase (SOD1) accumulates in vacuolated mitochondria in transgenic mice expressing amyotrophic lateral sclerosis-linked SOD1 mutations. *Acta Neuropathol.* **102**, 293–305.

33. Pardo, C. A., Xu, Z. S., Borchelt, D. R., Price, D. L., Sisodia, S. S. & Cleveland, D. W. (1995). Superoxide-dismutase is an abundant component in cell-bodies dendrites, and axons of motor-neurons and in a subset of other neurons. *Proc. Natl Acad. Sci. USA*, **92**, 954–958.

34. Okado-Matsumoto, A. & Fridovich, I. (2002). Amytrophic lateral sclerosis: a proposed mechanism. *Proc. Natl Acad. Sci. USA*, **99**, 9010–9014.

35. Elam, J. S., Taylor, A. B., Strange, R. W., Antonyuk, S. V., Doucette, P. A., Rodriguez, J. A. *et al.* (2003). Filamentous aggregates arise through gain-of interaction betwen SOD1 mutants linked to familial amytrophic lateral sclerosis. *Nature Struct. Biol.* In the Press.

36. Parge, H. E., Hallewell, R. A. & Tainer, J. A. (1992). Atomic structures of wild-type and thermostable mutant recombinant human Cu,Zn superoxide dismutase. *Proc. Natl Acad. Sci. USA*, **89**, 6109–6113.

37. Murshudov, G. N., Vagin, A. A. & Dodson, E. J. (1997). Refinement of macromolecular structures by the maximum-likelihood method. *Acta. Crystallog. sect. D*, **53**, 240–255.

38. Cardoso, R. M. F., Thayer, M. M., DiDonato, M., Lo, T. P., Bruns, C. K., Getzoff, E. D., Tainer, J. A. *et al.* (2002). Insights into Lou Gehrig's disease from the structure and instability of the A4V mutant of human Cu,Zn superoxide dismutase. *J. Mol. Biol.* **324**, 247–256.

39. Morris, A. L., MacArthur, M. W., Hutchinson, E. G. & Thornton, J. M. (1992). Stereochemical quality of protein structure coordinates. *Proteins: Struct. Funct. Genet.* **12**, 345–364.

40. Hart, P. J., Balbirnie, M. M., Ogihara, N. L., Nersissian, A. M., Weiss, M. E., Valentine, J. S. & Eisenberg, D. (1999). A structure based mechanism for copper–zinc superoxide dismutase. *Biochemistry*, **38**, 2167–2178.

41. Banci, L., Felli, I. C. & Kummerle, R. (2002). Direct detection of hydrogen bonds in monomeric superoxide dismutase: biological implications. *Biochemistry*, **41**, 2913–2920.

42. Sunde, M., Serpell, L. C., Bartlam, M., Fraser, P. E., Pepys, M. B. & Blake, C. C. F. (1997). Common core structure of amyloid fibrils by synchrotron X-ray diffraction. *J. Mol. Biol.* **273**, 729–739.

43. Pan, K. M., Baldwin, M., Nguyen, J., Gasset, M., Serban, A., Groth, D. *et al.* (1993). Conversion of alpha-helices into beta-sheets features in the formation of the scrapie prion proteins. *Proc. Natl Acad. Sci. USA*, **90**, 10962–10966.

44. Lindberg, M. J., Tibell, L. & Oliveberg, M. (2002). Common denominator of Cu/Zn superoxide dismutase mutants associated with amyotrophic lateral sclerosis: decreased stability of the apo state. *Proc. Natl Acad. Sci. USA*, **99**, 16607–16612.

45. Otwinowski, Z. & Minor, W. (1997). Processing of X-ray diffraction data collected in oscillation mode. In *Methods in Enzymology: Macromolecular Crystallography Part A* (Carter, C. W. & Sweet, R. M., eds), vol. 276, pp. 307–326, Academic Press, New York.

46. Vagin, A. A. & Teplyakov, A. (1997). MOLREP: an automated program for molecular replacement. *J. Appl. Crystallog.* **30**, 1022–1025.

47. Jones, T. A. (1978). A graphics model building and refinement system for macromolecules. *J. Appl. Crystallog.* **11**, 268–272.

48. Lamzin, V. S. & Wilson, K. S. (1993). Automated refinement of protein models. *Acta. Crystallog. sect. D*, **49**, 129–147.

49. Winn, M. D., Isupov, M. N. & Murshudov, G. N. (2001). Use of TLS parameters to model anisotropic displacements in macromolecular refinement. *Acta. Crystallog. sect. D*, **57**, 122–133.

50. Navaza, J. (1994). AMoRe: an automated package for molecular replacement. *Acta. Crystallog. sect. A*, **50**, 157–163.